(Received 11 March 2026, Accepted 17 April 2026, Scheduled 13 May 2026)

Whole Sub-7 GHz Four-Element Ultra-Wideband MIMO Antenna for IoT Applications Based on Characteristic Mode Theory

Chengzhu Du*, Xingyu Liu, Jiaxuan Tian, and Zhiyuan Wang

Faculty of Artificial Intelligence, Shanghai University of Electric Power, Shanghai 200090, China

ABSTRACT: This article describes a four-element ultra-wideband (UWB) Multiple-Input Multiple-Output (MIMO) antenna for the Sub-7 GHz. The antenna element is an elliptical patch slot antenna with a coplanar waveguide (CPW) feed. To make the bandwidth wider, we add step-by-step parasitic stubs based on the results of the Characteristic Mode Analysis (CMA) analysis, which can control multiple modes better. The four-element antenna is connected to a common ground structure with a central cross-shaped isolation stub and also inhibit the propagation of surface waves. It can be used in the range from 1.08 GHz to 8.70 GHz (155.8%), which is fabricated on a low-cost FR4 substrate. In this range, the isolation between antenna elements exceeds 20 dB. The performance of the design is very good. The envelope correlation coefficient (ECC) is less than 0.02, and the diversity gain (DG) is greater than 9.96.

1. INTRODUCTION

Mobile communication can evolve by relying on the deployment of a new spectrum and advanced system architectures that are the basis for improving user data rates [1]. The 5G capabilities should be extended, and the next 6G network is expected to support more Internet of Things (IoT) connections, especially the large-scale Internet of Things [2]. In 2022, 3GPP officially authorized the U6G spectrum (6425–7125 MHz). This marks it as a potential spectrum for future communication systems [3]. Modern IoT devices typically need to operate across multiple frequency bands, such as GNSS, LoRa, Zigbee, Bluetooth, and Wi-Fi [4–6]. The above wireless communication frequency bands cover applications in both urban and remote areas, such as mobile devices, urban traffic, autonomous driving, low-altitude UAVs, medical emergency response, open-sea navigation, and smart grids. In addition, 6G can transmit wireless energy, which will bring new methods to a large number of future IoT devices [7]. These frequency bands are mainly in the sub-7 GHz range. A high-speed broadband wireless network is limited, and Multiple-Input Multiple-Output technology can solve this problem [8]. Therefore, combining MIMO and ultra-wideband sub-7 GHz technology makes sense for the development of future large-scale IoT applications.

As wireless communication networks advance, IoT devices are becoming smaller and more integrated. This makes improving isolation between antenna elements in MIMO systems a key research focus. For example, ref. [9] places two 1×4 arrays facing each other and uses a neutralization line structure. This configuration not only suppresses surface wave propagation but also reduces mutual coupling between MIMO elements, thereby enhancing the isolation to -20 dB. Ref. [10] proposes a rectangular patch antenna based on a fractal structure, which utilizes an inverted T-shaped stub between two parallel antennas to improve isolation from -13.6 dB to -21 dB. In [11], a decoupling method suitable for slot antennas was proposed. By etching an open-ended slot and incorporating a 3T-shaped strip, the isolation was improved from -14 dB to -20 dB. In [12], an EBG structure was integrated into an X-shaped stub, which successfully enhanced both the impedance matching and isolation of a four-element UWB antenna. It is noteworthy that this structure was not connected to the ground plane. A Vias-Based Coupling Current Steering (VBCCS) structure was proposed in [13], which enhanced the isolation to 17 dB.

In recent years, antenna design with characteristic mode analysis (CMA) has grown significantly [14–25], making it a powerful tool for antenna engineers. Notably, the CMA is independent of feed configuration, allowing it to focus squarely on the analysis of the antenna structure itself [16]. For UWB antennas, studying the surface current distribution through characteristic modes helps to design for wideband performance. In [19], the CMA of the initial antenna design identified the root cause of the poor low-frequency response: although Mode 4 resonated at 3.2 GHz, it exhibited poor excitability. The targeted integration of a T-stepped stub with an EBG structure reconfigured the modal distribution. This intervention successfully tuned Mode 5 to radiate effectively at 3 GHz while shifting Mode 4 higher, thereby extending the impressive impedance bandwidth to 3.07–11.1 GHz (113.34%) for complete UWB coverage. In [20], the relationship between the Modal Significance at each stage and frequency variation is demonstrated, which intuitively reflects which modes are excited in which frequency bands, thereby explaining the process of bandwidth expansion. The study in [22] manages and adjusts the characteristic mode distribution throughout the antenna's evolution, effectively extending the bandwidth of the UWB-MIMO antenna. Using an FR4 substrate, this method achieves a 126.4%

* Corresponding author: Chengzhu Du (duchengzhu@163.com).

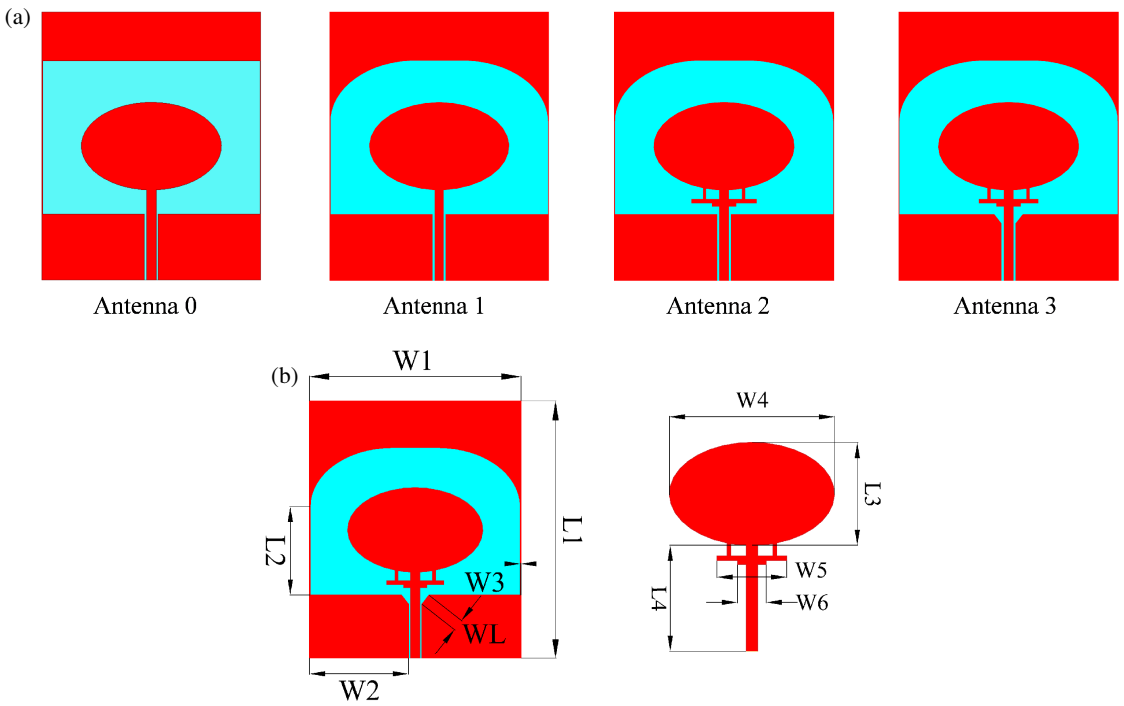

FIGURE 1. Structural layout of the antenna element. (a) The iterative development of the antenna element. (b) The finalized geometric configuration of the antenna element.

bandwidth. Similarly, the design in [24] incorporates resonant rings inspired by metamaterials to widen the bandwidth. Its unique aspect, however, is the use of Characteristic Mode Analysis, which shows a notable rise in the number of characteristic modes. This creates a group of tightly packed resonant modes that together produce a continuous wideband response from 3.3 to 13.84 GHz (123%). All of the above antennas are analyzed using characteristic mode theory for microstrip broadband antennas, while there is relatively little research on characteristic mode theory for broadband antennas based on CPW-fed types. Therefore, based on characteristic mode analysis, it is a challenging task to design a UWB-MIMO antenna covering 1–8 GHz with high isolation.

This article describes a UWB-MIMO antenna for sub-7 GHz applications. The antenna is made on an FR4 substrate; the size of the substrate is 130 mm × 130 mm × 0.8 mm; the operating frequency is from 1.08 GHz to 8.70 GHz; and the isolation between the antennas is greater than 20 dB.

2. THE PROPOSED ANTENNA DESIGN

2.1. Antenna Element

Figure 1 outlines how the antenna was developed, along with the geometry of the antenna's final component. In the first step of the design process, Antenna 0 is an elliptical monopole with a CPW feed. In the second step, Antenna 1 has optimized the impedance matching by adding the curved branch at the top. In the third step, stepped parasitic stubs were integrated along the lower edge of the elliptical patch to form Antenna 2. For Antenna 3, the ground plane's corners were truncated, which can achieve better impedance matching performance. The fully refined antenna component was built on an FR4 substrate measuring 54 mm × 66 mm × 0.8 mm, and this substrate has a relative permittivity of 4.4 and a loss tangent value of 0.02. For the finished layout of this antenna, we used the following geometric parameters: $W1 = 54$ mm, $L1 = 66$ mm, $W2 = 24.6$ mm, $W3 = 0.6$ mm, $W4 = 34$ mm, $W5 = 14.5$ mm, $W6 = 6$ mm, $L2 = 21.8$ mm, $L3 = 20.6$ mm, $L4 = 22$ mm.

The S-parameters corresponding to the antenna element are presented in Fig. 2. The bandwidth of Antenna 0 is 1.45–1.75 GHz. With a curved branch at the top, Antenna 1 has a wider bandwidth of 1.4–1.9 GHz. With the loading of the stepped parasitic stubs, the impedance matching of Antenna 2 at high frequencies is significantly improved. Antenna 3 is the proposed antenna element with a frequency bandwidth extending from 1.41 GHz to 7.66 GHz.

2.2. Effect of the Stepped Parasitic Stubs

With the help of the Characteristic Mode Analysis, Modal Significance (MS) and Characteristic Angle (CA) are important analysis parameters. MS is computed by Equation (1). From this equation, it can be shown that n is the mode index, and λ_n represents the corresponding eigenvalue. A mode resonates in a certain frequency range, when its MS_n exceeds 0.707. Additionally, when an MS value is approaching 1, it shows that the corresponding mode has more excitability.

$$MS_n = \left| \frac{1}{1 + j\lambda_n} \right| \tag{1}$$

CA can be calculated by Equation (2), reflecting the radiating efficiency of a mode. A characteristic angle near 180° denotes

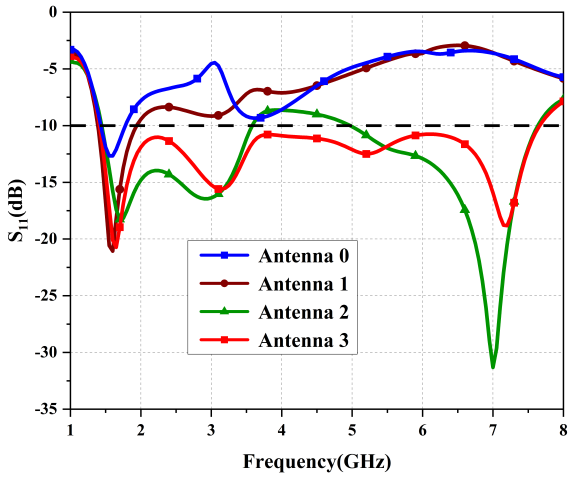

FIGURE 2. S_{11} in different design stages.

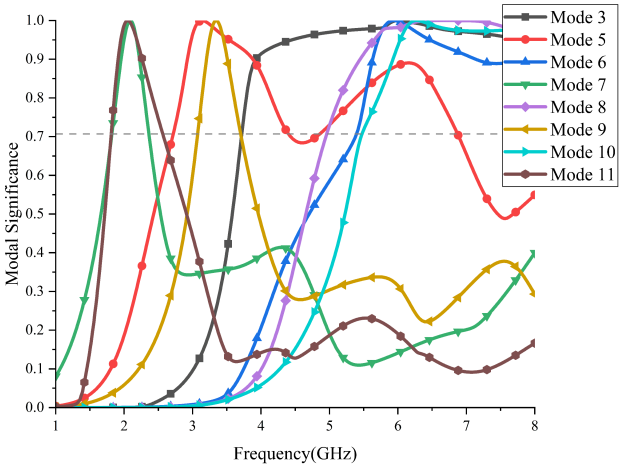

FIGURE 3. MS of the eight modes for Antenna 1.

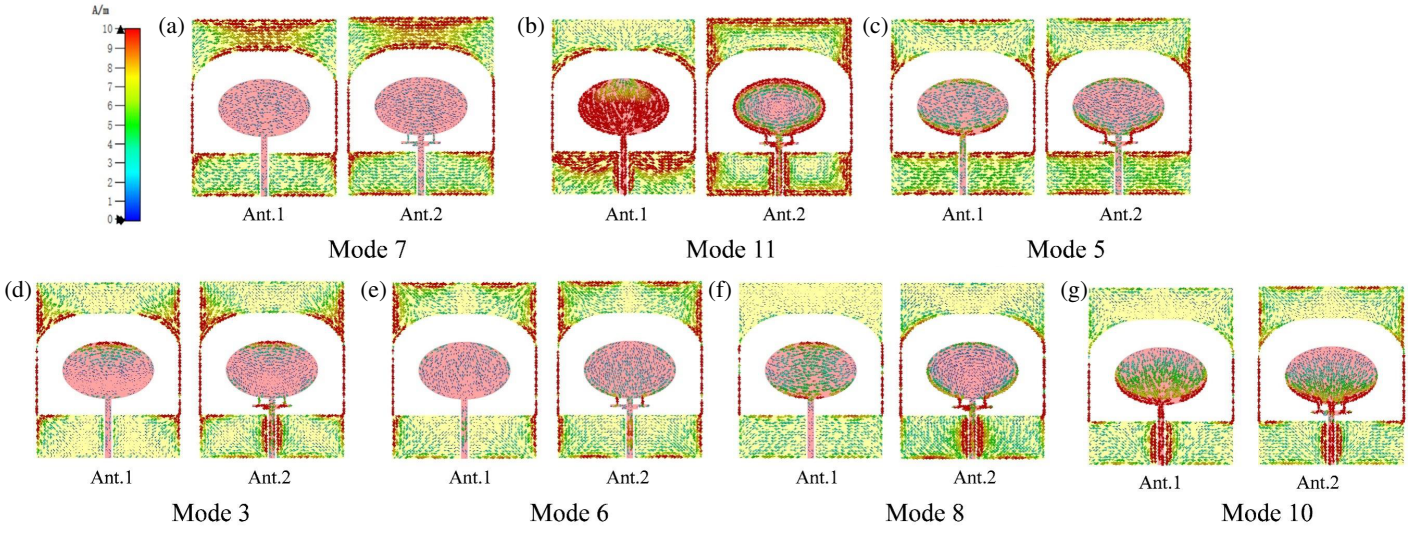

FIGURE 4. The surface current distributions of Antenna 1 and Antenna 2: (a) Mode 7 at 1.5 GHz, (b) Mode 11 at 1.5 GHz, (c) Mode 5 at 3 GHz, (d) Mode 3 at 6 GHz, (e) Mode 6 at 6 GHz, (f) Mode 8 at 6 GHz, (g) Mode 10 at 6 GHz.

that the mode is in a strong radiating state.

$$\alpha_n = 180^\circ - \tan^{-1}(\lambda_n) \tag{2}$$

As shown in Fig. 2, Antenna 1 resonates only at lower frequencies. To extend the antenna's bandwidth, the antenna element is analyzed via Characteristic Mode Theory. Fig. 3 presents the MS results of Antenna 1, derived via the commercial simulation tool CST. From this figure, it can be seen that the lower frequency band of the antenna is dominated mainly by Modes 7 and 11, while the higher band is governed by Modes 3, 6, 8, and 10. In the mid-band, however, Mode 5 emerges as the dominant mode because Mode 9 exhibits a narrower bandwidth and a higher Q-factor in comparison.

As can be seen in Fig. 4, at 1.5 GHz, the surface current distribution of Mode 7 on the feed line remains unchanged, while the current distribution around the ground plane of Mode 11 is enhanced. In Mode 5 at 3 GHz, the surface current spreads to the parasitic stub, optimizing the impedance matching near 3 GHz band. At 6 GHz, the current distribution of Modes 8 and 10 on the feed line and the nearby ground plane is enhanced, but at this time, impedance mismatch occurs at the high frequency of Ant. 2. Therefore, slotting can be chosen in this area.

It is noteworthy that the introduction of a stepped parasitic stub affects the current distribution of the modes at the feed line. This offers a twofold benefit: first, it creates conditions for exciting higher-order modes; second, it permits the truncation of corners on the ground plane near the feed line to further optimize impedance matching. This approach constitutes the improvement implemented in Antenna 3. The effect of dimensional changes of $W5$ and $W6$ in the stepped parasitic stub on S_{11} is shown in Fig. 5. As can be seen from the figure, variations in $W5$ and $W6$, which are key parameters of the stepped parasitic stub, have a significant impact on the impedance matching at middle and high frequencies, and conversely, their effect on the low-frequency impedance matching is relatively minor.

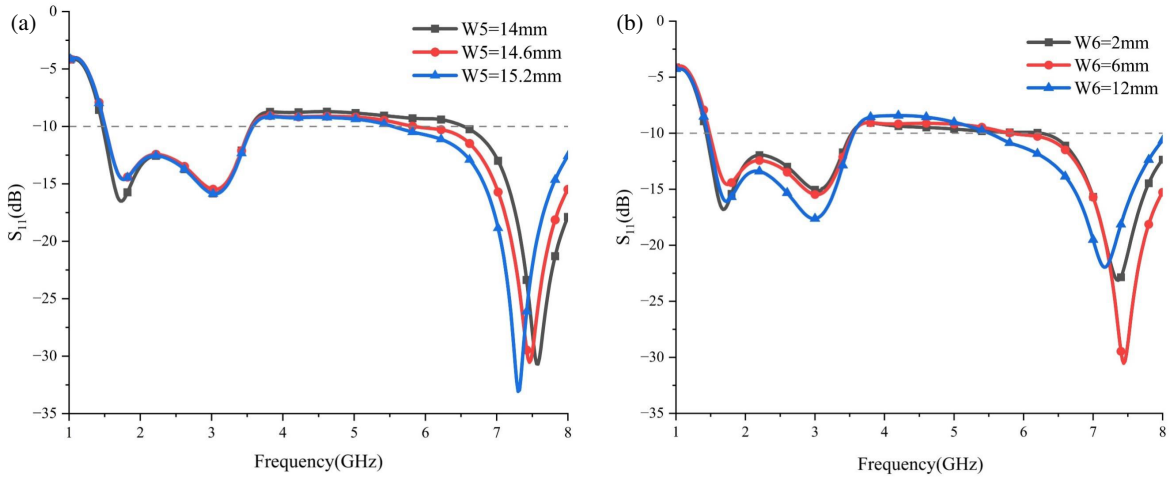

FIGURE 5. Simulated S_{11} for the effect of the stepped parasitic stub.

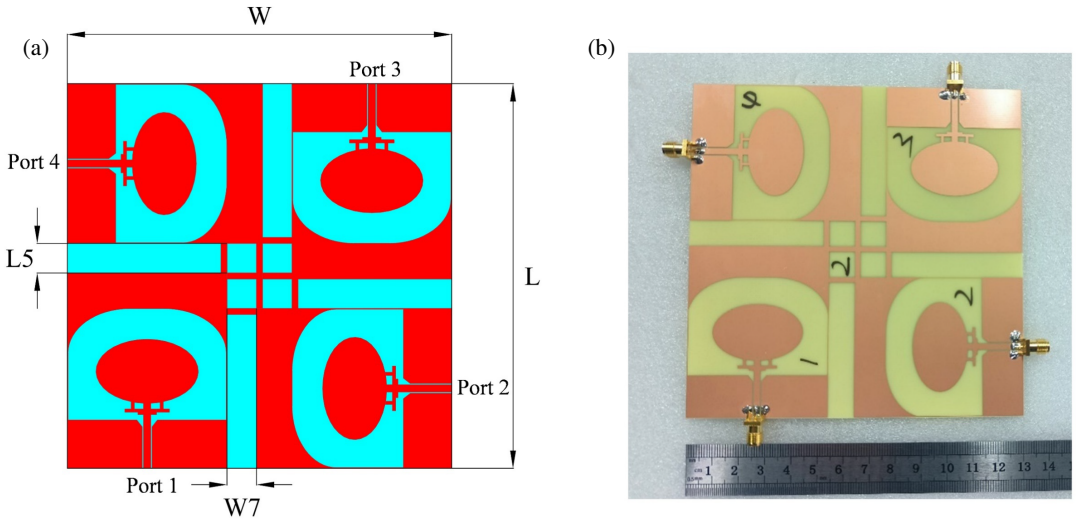

FIGURE 6. The simulation model and fabricated prototype of the four-element antenna. (a) The structure of the four-element antenna. (b) The fabricated four-element antenna.

2.3. Four-Element Antenna

Figure 6 presents the simulation model and physical prototype of the four-element antenna. The proposed antenna adopts the CPW feeding method and is fabricated on an FR4 substrate with dimensions of 130 mm × 130 mm × 0.8 mm. The antenna elements are arranged orthogonally, and an isolation stub is positioned at the antenna's center to enhance isolation performance. For the finalized design of the antenna, the geometric parameters (derived via simulation and optimization) are as follows: $L = 130$ mm, $W = 130$ mm, $L5 = 2$ mm, $W7 = 2$ mm.

2.4. Decoupling Structure Analysis

Figure 7 illustrates the evolution process of the decoupling structure. The first design comprises a four-element MIMO antenna in an orthogonal configuration. The subsequent design incorporates rectangular stubs to interconnect all four antenna elements, serving to establish a unified reference potential plane and ensure the stability of the excitation modes. Finally, a cross-shaped isolation stub is employed for enhanced isolation.

Figure 8 depicts the S-parameter evolution of the four-element MIMO antenna. For Antenna I, the operating bandwidth spans 1.41–6.12 GHz. As observed in this figure, connecting the ground expands Antenna II's bandwidth to 1.08–6.42 GHz. This aligns with prior modal analysis, which identifies Modes 7 and 11 as lower-frequency dominant modes, and shows that the stubs extend these modes' current path along the ground plane's edge. With the integration of cross stubs, Antenna III undergoes impedance matching optimization in the 6.12–6.54 GHz high-frequency band, resulting in a final operating bandwidth of 1.08–8.7 GHz.

The introduction of the isolation stub significantly enhanced the isolation at mid and high frequencies. In the evolution of the antenna, the values of S_{21} within the 4–7 GHz range and S_{31} within the 5–8 GHz range have both been significantly reduced. Ultimately, the achieved isolation across the entire operating band is better than 20 dB for the final design.

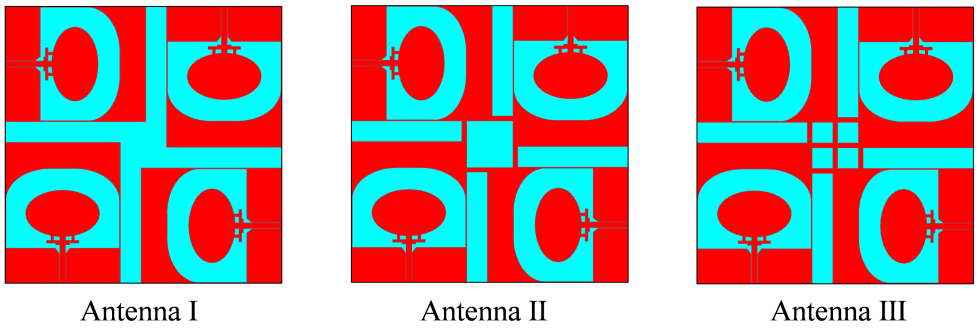

FIGURE 7. The evolution process of the four-element antenna.

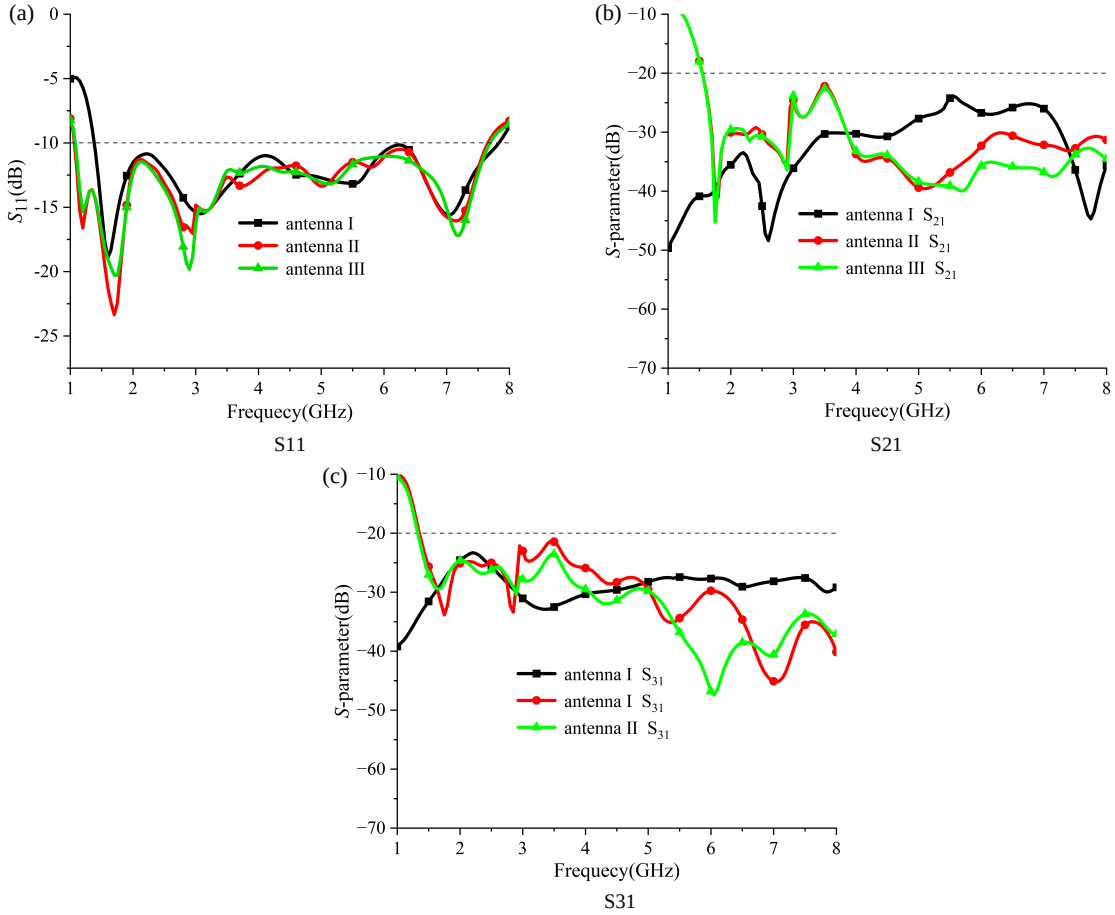

FIGURE 8. S_{11}, S_{21}, and S_{31} in different design stages of the four-element antenna.

The effectiveness of the isolation structure is confirmed by the current distributions in Fig. 9. At 3.5, 4.7, and 6.5 GHz, with only Port 1 excited, the surface currents are strongly localized on the driven element and the isolation branch itself, while being suppressed elsewhere. This effectively minimizes the coupling between the antenna units.

3. RESULTS AND DISCUSSION

3.1. S-Parameter

The four-element ultra-wideband antenna was prototyped and characterized. Fig. 10 compares the simulated and measured performance results. As shown in Fig. 10(a), the measurement results indicate the antenna's operating bandwidth spans 1.08–8.70 GHz. Correspondingly, Fig. 10(b) demonstrates that both simulated and measured isolations exceed 20 dB across the full operating band. Due to fabrication tolerances, material losses, and measurement environment effects, there are some discrepancies between the simulated and measured curves, but the results still satisfy the design requirements.

3.2. Radiation Patterns at Different Frequencies

Figure 11 presents simulated and measured normalized radiation patterns (covering E- and H-planes) at 3, 5, and 7 GHz,

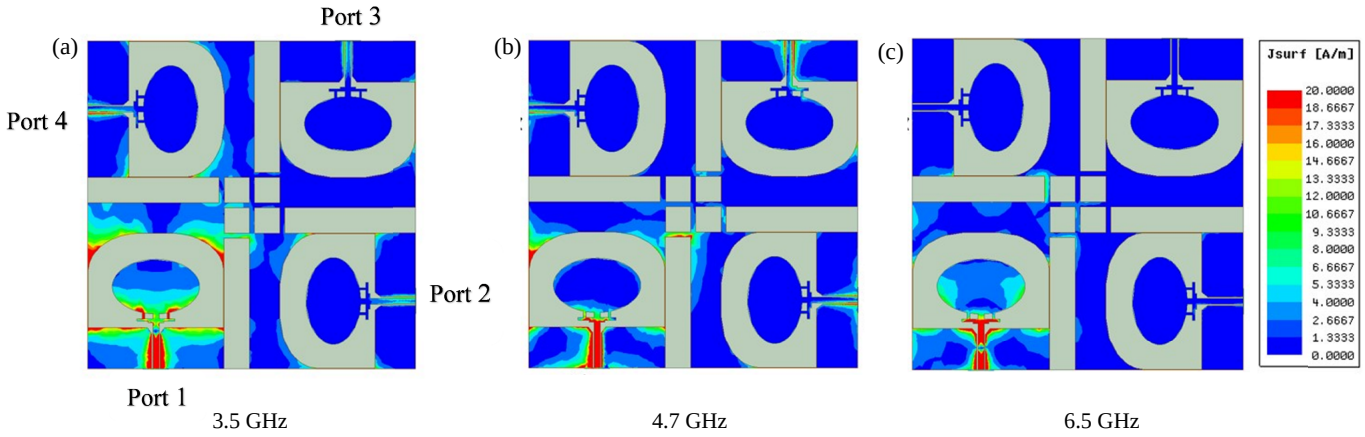

FIGURE 9. Surface current distributions at different frequencies.

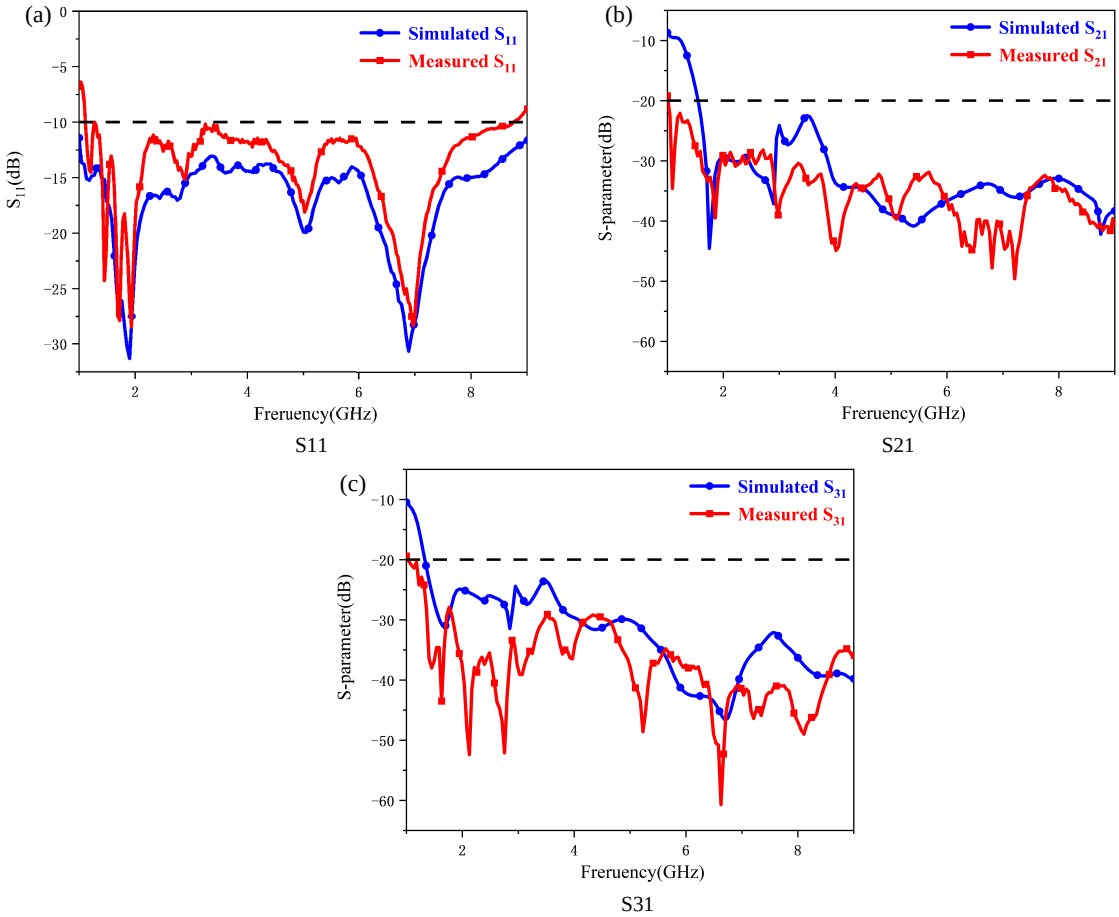

FIGURE 10. The simulated and measured S-parameters.

with good overall consistency. These patterns verify the E-plane bidirectional radiation characteristic and H-plane omnidirectional radiation characteristic of the designed antenna. While minor distortions appear in the 7 GHz patterns, they do not notably degrade the antenna's key transceiving performance.

3.3. Gain

Figure 12 compares the simulated and measured peak gains of the proposed antenna. The measured peak gains of the final designed antenna are 3.3 dB at 2 GHz, 6.5 dB at 5 GHz, and 6.5 dB at 8 GHz.

3.4. Envelope Correlation Coefficient and Diversity Gain

The envelope correlation coefficient (ECC) is a key metric for evaluating MIMO diversity performance, as it quantifies the correlation between antenna elements: lower ECC corresponds to weaker inter-element correlation and superior MIMO performance. Diversity gain (DG) is another core indicator. The typical design criteria is that ECC < 0.5 and DG close to 10. As

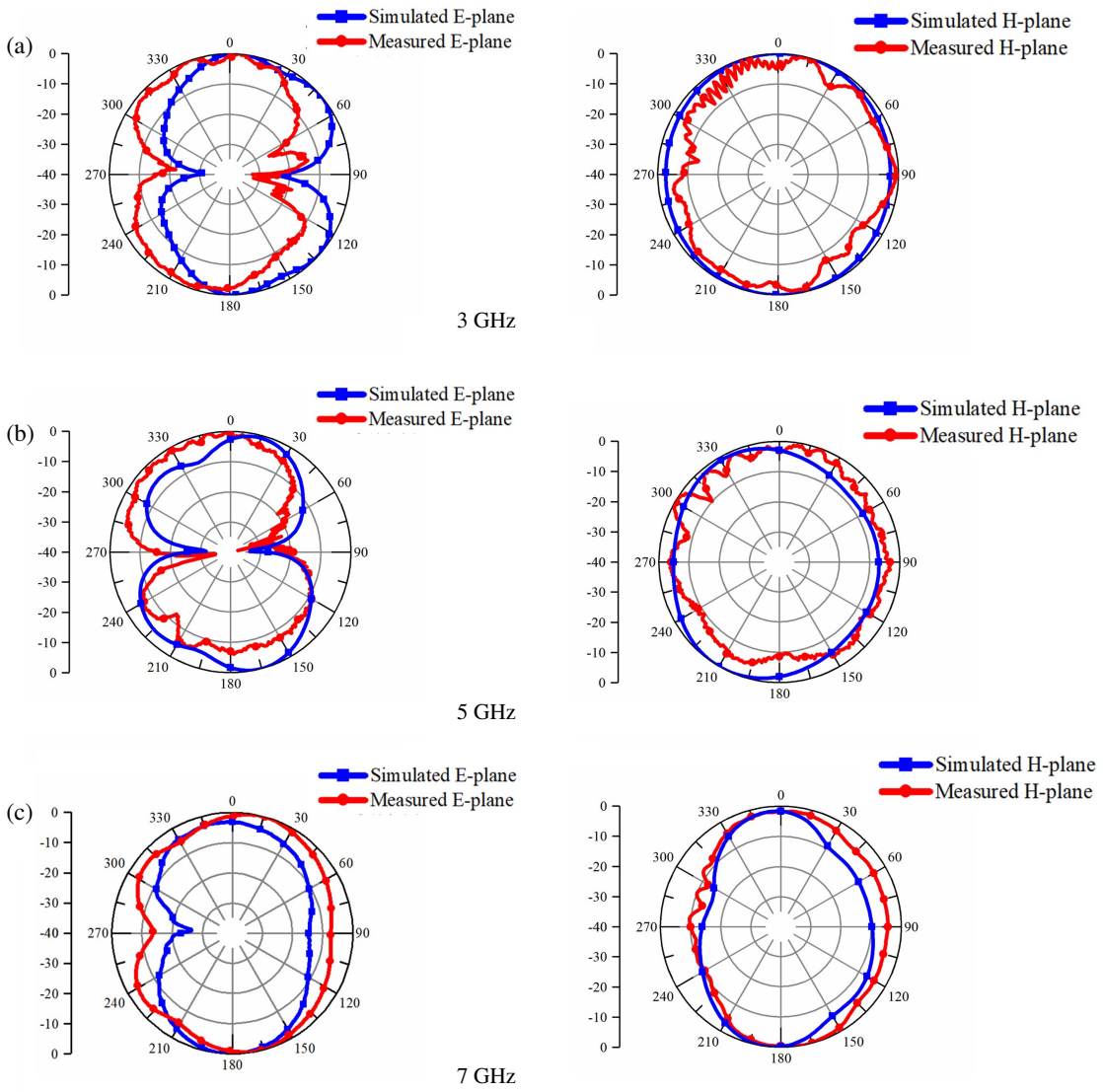

FIGURE 11. Radiation patterns of the presented antenna.

shown in Fig. 13, the proposed antenna achieves a notably low ECC (< 0.02) across target bands. Moreover, Fig. 14 illustrates that the calculated DG exceeds 9.996 across all operating bands, confirming strong diversity capability. ECC is computed from the antenna's far-field data [26]. Formula 3 is used for calculating the ECC of the antenna, where $F(\theta, \varphi)$ represents the vector wave function in different directions. The diversity gain is derived from the standard formula (4) [27].

$$\rho_e(i,j) = \frac{\left|\iint_{4\pi} \vec{F}_i(\theta,\varphi) \cdot \vec{F}_j(\theta,\varphi)\, d\Omega\right|^2}{\iint_{4\pi} \left|\vec{F}_i(\theta,\varphi)\right|^2 d\Omega \cdot \iint_{4\pi} \left|\vec{F}_j(\theta,\varphi)\right|^2 d\Omega} \quad (3)$$

$$DG = 10\sqrt{1-(ECC)^2} \quad (4)$$

3.5. Total Active Reflection Coefficient

The total active reflection coefficient (TARC) is very important for evaluating the performance of MIMO systems. To investigate the characteristics of the proposed four-port MIMO antenna in this article, TARC was measured under four different excitation phases (0°, 60°, 120°, and 180°). Fig. 15 shows that the measured TARC remains below -10 dB across all operating bands for these phase states, demonstrating stable and good MIMO performance. The concept of TARC for MIMO systems is discussed in [28], where N represents the total number of ports, S the scattering parameter, and θ the phase.

$$TARC = N^{-0.5}\sqrt{\sum_{i=1}^{N}\left|\sum_{k=1}^{N} S_{ik} e^{j\theta_{k-1}}\right|^2} \quad (5)$$

3.6. Performance Comparison

The performance comparison is concluded in Table 1. Refs. [9–11, 19] all present two-element MIMO UWB antenna designs, which are insufficient to meet the information transmission rate demands of large-scale IoT. Among them, only [19] employs Characteristic Mode Analysis to elucidate the physical radiation mechanisms of the antenna; however, its rela-

TABLE 1. Comparison of antenna performance.

Ref.	No. of ports	Size (mm)	CMA	Bandwidth (GHz)	Fractional Bandwidth	Feed Method	Ground connection	Isolation (dB)	ECC	DG
[9]	2	$140 * 135 * 1.6$	No	3.01–6.5	73.4%	Microstrip	Yes	20	< 0.02	10
[10]	2	$20 * 34 * 1.6$	No	2.34–14.06	143%	CPW	Yes	21	0.003	9.96
[11]	2	$257 * 257 * 1.5$	No	0.63–6	162%	Microstrip	Yes	20	< 0.005	/
[19]	2	$27 * 22 * 0.8$	Yes	3.07–11.1	113.3%	Microstrip	Yes	20	0.05	9.986
[20]	4	$40 * 40 * 1.6$	Yes	3.1–11	112.1%	Microstrip	No	26	0.0016	9.99
[22]	4	$28 * 40 * 1.6$	Yes	3.1–13.75	126.4%	Microstrip	No	25	0.0045	9.982
[24]	4	$73 * 73 * 1.6$	Yes	3.3–13.84	123%	Microstrip	Yes	14	0.2	/
Prop.	4	$130 * 130 * 0.8$	Yes	1.08–8.7	155.8%	CPW	Yes	20	0.02	9.996

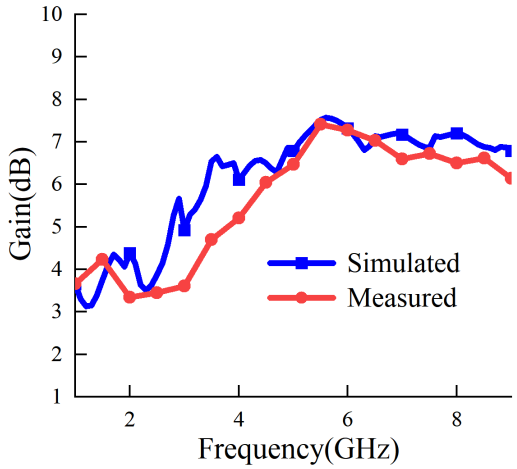

FIGURE 12. Gain of the presented antenna.

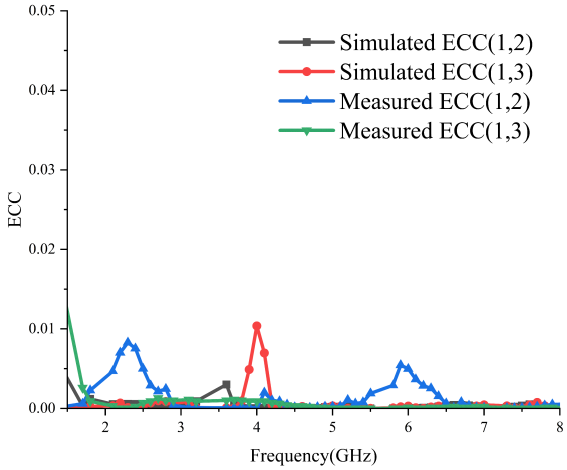

FIGURE 13. ECC of the presented antenna.

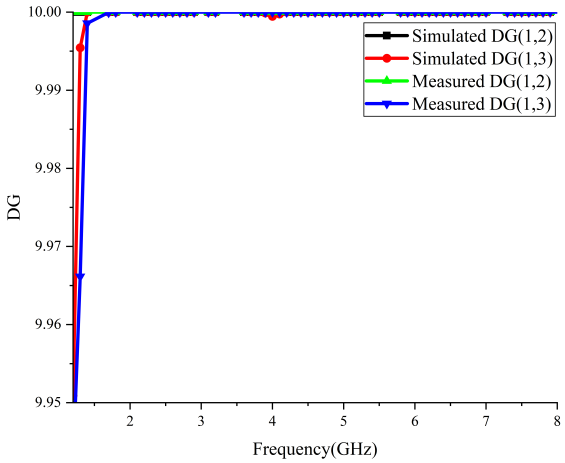

FIGURE 14. DG of the presented antenna.

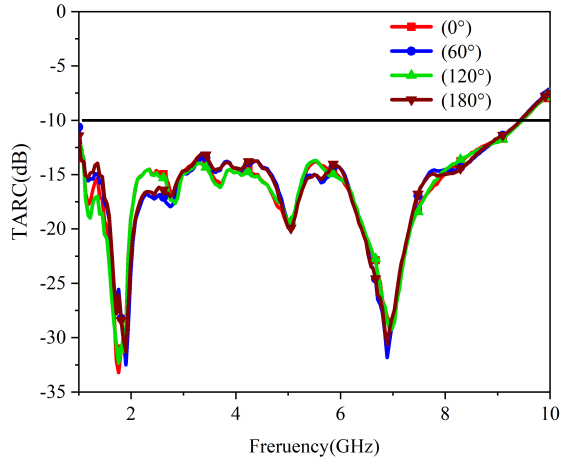

FIGURE 15. TARC of the presented antenna.

tive bandwidth is limited to 113.3%. Refs. [20, 22, 24] conduct mode analysis based on four-element broadband antennas; yet their achieved relative bandwidths remain lower than that of the MIMO antenna proposed in this work. By implementing a ground connection structure, our design enhances the relative bandwidth to 155.8% and improves isolation to 20 dB. Furthermore, we utilize CMA to provide a detailed analysis of the bandwidth extension mechanism for antennas with CPW feeding.

4. CONCLUSION

In this article, we design and prototype a four-element UWB-MIMO antenna for the sub-7 GHz band. This antenna achieves an operating bandwidth of 1.08–8.70 GHz, adopting a CPW-fed structure with interconnected ground planes and a central cross-shaped isolation stub. Port isolation exceeding 20 dB is realized over the full operating band. The wide-band design process was guided by Characteristic Mode Analysis. Through analyzing the current distribution characteristics of each mode, this work manipulates the distributions of multiple modes with stepped parasitic stubs. Ultimately, we achieved the desirable bandwidth performance. Besides, the antenna shows good diversity performance with ECC below 0.02 and DG exceeding 9.996. The ultra-wideband antenna designed in this paper can meet the communication requirements of various frequency bands for IoT devices. However, for the future upgrade of a large number of IoT devices, the size of the antenna needs to be reduced to facilitate more compact deployment.

REFERENCES

[1] Wong, K.-L., C.-Y. Wu, W.-T. Li, and W.-Y. Li, "Hybrid MIMO antennas comprising ultra-wideband frame conjoined two-antenna elements in 3.3–8.4 GHz and low-profile backcover four-antenna module in 6.425–8.4 GHz for 5G/6G smartphones," *IEEE Access*, Vol. 13, 91 611–91 624, 2025.

[2] Guo, F., F. R. Yu, H. Zhang, X. Li, H. Ji, and V. C. M. Leung, "Enabling massive IoT toward 6G: A comprehensive survey," *IEEE Internet of Things Journal*, Vol. 8, No. 15, 11 891–11 915, 2021.

[3] Li, M., W. Xu, Z. Hu, and A. Liu, "A wideband CSI feedback scheme based on loewner interpolation and model order reduction," *IEEE Wireless Communications Letters*, Vol. 14, No. 11, 3749–3753, 2025.

[4] Khan, S., T. Mazhar, T. Shahzad, A. Bibi, W. Ahmad, M. A. Khan, M. M. Saeed, and H. Hamam, "Antenna systems for IoT applications: A review," *Discover Sustainability*, Vol. 5, No. 1, 412, 2024.

[5] Du, C. and Y. Ren, "A CPW-fed wideband four-port MIMO slot antenna with high isolation for sub-6G applications," *Journal of Electromagnetic Waves and Applications*, Vol. 38, No. 4, 428–442, 2024.

[6] Gupta, N. and M. E. Bakkali, "A compact meander line-based wideband patch antenna for vehicle-to-vehicle and WLAN applications," *Measurement*, Vol. 256, 118295, 2025.

[7] López, O. L. A., H. Alves, R. D. Souza, S. Montejo-Sánchez, E. M. G. Fernández, and M. Latva-Aho, "Massive wireless energy transfer: Enabling sustainable IoT toward 6G era," *IEEE Internet of Things Journal*, Vol. 8, No. 11, 8816–8835, 2021.

[8] Raj, T., R. Mishra, P. Kumar, and A. Kapoor, "Advances in MIMO antenna design for 5G: A comprehensive review," *Sensors*, Vol. 23, No. 14, 6329, 2023.

[9] Ahmed, H., A. M. Ameen, A. Magdy, A. Nasser, and M. Abo-Zahhad, "A sub-6 GHz two-port crescent MIMO array antenna for 5G applications," *Electronics*, Vol. 14, No. 3, 411, 2025.

[10] Sediq, H. T., "Miniaturized MIMO antenna design based on octagonal-shaped SRR metamaterial for UWB applications," *AEU — International Journal of Electronics and Communications*, Vol. 172, 154946, 2023.

[11] Chen, G. R., L. H. Ye, H. Jiang, X. Tian, Z. Hu, and J.-F. Li, "Compact ultrawideband MIMO slot antenna with high isolation," *International Journal of Communication Systems*, Vol. 37, No. 10, e5781, 2024.

[12] Khattak, R. Y., Q. Ahmed, S. Shoaib, P. I. Lazaridis, and I. Ahmed, "Design and performance investigation of an ultra-thin and flexible polyimide-based UWB antenna," *Results in Engineering*, Vol. 27, 105956, 2025.

[13] Singh, H. V. and S. Tripathi, "Compact UWB MIMO antenna with Fork-shaped stub with vias based coupling current steering (VBCCS) to enhance isolation using CMA," *AEU — International Journal of Electronics and Communications*, Vol. 129, 153550, 2021.

[14] Lai, Q. X., Y. M. Pan, and S. Y. Zheng, "A self-decoupling method for MIMO antenna array using characteristic mode of ground plane," *IEEE Transactions on Antennas and Propagation*, Vol. 71, No. 3, 2126–2135, 2023.

[15] Zhao, X., S. P. Yeo, and L. C. Ong, "Planar UWB MIMO antenna with pattern diversity and isolation improvement for mobile platform based on the theory of characteristic modes," *IEEE Transactions on Antennas and Propagation*, Vol. 66, No. 1, 420–425, 2018.

[16] Adams, J. J., S. Genovesi, B. Yang, and E. Antonino-Daviu, "Antenna element design using characteristic mode analysis: Insights and research directions," *IEEE Antennas and Propagation Magazine*, Vol. 64, No. 2, 32–40, 2022.

[17] Liu, H., Z. Yang, B. Zhang, Y. Gao, L. Dong, Y. Bai, C. Feng, and W. Hu, "Broadband metasurface antenna optimized for high-frequency radiation patterns using characteristic mode analysis," *International Journal of Antennas and Propagation*, Vol. 2025, No. 1, 5569883, 2025.

[18] Naik, D. K., D. C. Panda, R. Swain, A. Muduli, and A. Pal, "Characteristic mode inspired broadband circularly polarized metasurface antenna with triple-mode excitation for sub-6 GHz applications," *Scientific Reports*, Vol. 15, No. 1, 33965, 2025.

[19] Li, W., L. Wu, S. Li, X. Cao, and B. Yang, "Bandwidth enhancement and isolation improvement in compact UWB-MIMO antenna assisted by characteristic mode analysis," *IEEE Access*, Vol. 12, 17 152–17 163, Jan. 2024.

[20] Suresh, A. C., C. Althi, C. G, O. P. Kumar, M. Alathbah, and B. Madhav, "Modal analysis-based ultrawideband 4 × 4 MIMO antenna with flower configuration," *AEU — International Journal of Electronics and Communications*, Vol. 192, 155685, 2025.

[21] Raut, B., B. K. Santi, R. Swain, D. C. Panda, and D. K. Naik, "Characteristic mode inspired compact broadband circularly polarized non-uniform metasurface antenna for sub-7 GHz applications," *AEU — International Journal of Electronics and Communications*, Vol. 200, 155939, 2025.

[22] Suresh, A. C., T. S. Reddy, B. T. P. Madhav, S. Das, S. Lavadiya, A. D. Algarni, and W. El-Shafai, "Investigations on stub-based UWB-MIMO antennas to enhance isolation using characteristic mode analysis," *Micromachines*, Vol. 13, No. 12, 2088, 2022.

[23] Li, X., Z. Zhou, K. Wang, Y. Yang, Z. Pang, X. Zhou, W. Tang, Z. Huang, and D. Lan, "UWB metasurface antenna with improved gain and bandwidth for WBAN application," *IEEE Transactions on Consumer Electronics*, Vol. 71, No. 2, 5465–5474, 2025.

[24] Chaudhary, P., A. Kumar, R. K. Arya, and M. Ali, "Metamaterial-inspired UWB MIMO antenna with polarization diversity," *AEU — International Journal of Electronics and Communications*, Vol. 187, 155518, 2024.

[25] Xiao, B. and H. Wong, "Whole sub-6 GHz multiorder-dual-degenerate-modes loop antenna in mobile smart devices for IoT applications," *IEEE Internet of Things Journal*, Vol. 12, No. 16, 33 144–33 154, 2025.

[26] Nikam, P. B., J. Kumar, V. Sivanagaraju, and A. Baidya, "Dual-band reconfigurable EBG loaded circular patch MIMO antenna using defected ground structure (DGS) and PIN diode integrated branch-lines (BLs)," *Measurement*, Vol. 195, 111127, 2022.

[27] Perli, B. R., T. Addepalli, A. K. Sohi, S. Medasani, M. Sharma, I. M. Ibrahim, and A. J. A. Al-Gburi, "Design and Theory of Characteristic Mode Analysis (TCMA) of 4 × 4 high isolation MIMO antenna for sub-6 GHz 5G communications," *Results in Optics*, Vol. 21, 100903, 2025.

[28] Gollamudi, N. K., Y. V. Narayana, and A. M. Prasad, "Compact and asymmetric fed modified hexagonal shaped multiple-input multiple-output (MIMO) antenna for 5G sub: 6 GHz (N77/N78 & N79) and WLAN applications," *Analog Integrated Circuits and Signal Processing*, Vol. 114, No. 1, 103–112, 2023.